Ecotoxicology and Environmental Safety 236 (2022) 113496

Contents lists available at ScienceDirect

Ecotoxicology and Environmental Safety

journal homepage: www.elsevier.com/locate/ecoenv

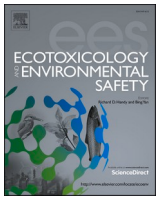

Increase in fluoride concentration in mine water in Shendong mining area, Northwest China: Insights from isotopic and geochemical signatures

Chunming Hao [a,b,1], Ximeng Sun [a], Bing Xie [a], Shuanglin Hou [c,d,*]

[a] North China Institute of Science and Technology, Hebei 065201, PR China
[b] State Key Laboratory of Groundwater Protection and Utilization by Coal Mining, Beijing 100011, PR China
[c] Hebei Key Laboratory of geological resources and environment monitoring and protection, Hebei 050011, PR China
[d] Hebei Geo-Environment Monitoring, Hebei 050011, PR China

ARTICLE INFO

Edited by Dr. Hao Zhu

Keywords:
Fluoride
Isotopes
Mining activities
Ion exchange
Competitive effect

ABSTRACT

Mine water poses severe threats to the quality of the water supply and ecological environment of the Shendong mining areas owing to its excessive fluoride (F^-) content. However, the geochemical behaviours and enrichment mechanisms responsible for F^- enrichment during mining activities are not fully understood. In total, 18 Yanan groundwater and 45 mine water samples were collected to analyse the spatial distribution, hydrogeochemical behaviours, and formation mechanisms related to elevated F^- levels by analysing the stable isotopes and water-rock interactions. In this study, F^- concentrations in mine water samples varied from 0.16 to 12.75 mg/L, with a mean value of 6.10 mg/L, and 77.78% of the mine water samples had a concentration that exceeded China's national standards (1.00 mg/L) for drinking water. The F^- concentration was markedly high in the mine water samples, with the mean F^- concentration being 1.58 times of that in the Yanan groundwater samples. The results of stable isotopes ($^{18}O_{H2O}$, D, $^{34}S_{SO4}$, and $^{18}O_{SO4}$) and water-rock interaction analyses suggested that cation exchange and competitive effects were the dominant factors responsible for elevated F^- concentration in mine water during mining activities. Thus, the weathering of F-bearing minerals, agriculture, and domestic activities do not play a significant role in the secondary enrichment of F^- concentration.

1. Introduction

Fluorine (F) is one of the lightest halogen elements, and fluoride (F^-) is an abundant trace element in the air, soil, and water (Ali et al., 2018; Dehbandi et al., 2018; Chen et al., 2021). F^- is an important component of natural water and an essential element for life; however, its optimal concentration should be between that of beneficial intake and toxic exposure (Currell et al., 2011; Deng et al., 2011; Emenike et al., 2018). In children, F^- exposure of 0.05–0.07 mg/kg body weight/day is optimal for dental health benefits (J. He et al., 2013; X. He et al., 2013; Aghapour et al., 2018; Kalpana et al., 2019). However, a high intake of F^- (> 1.50 mg/L) in drinking water for a prolonged period leads to diseases (Battaleb et al., 2013; Rafique et al., 2015; Olaka et al., 2016). For example, ingestion of 1.50–5.00 mg/L, 5.00–10.00 mg/L, and > 10.00 mg/L of F^- via drinking water may result in dental fluorosis (Aghapour et al., 2018; Toolabi et al., 2021), skeletal deformities (Goodarzi et al., 2017; Yousefi et al., 2018), arthritis, neurological disorders, thyroid disorders, cancer, infertility, and hypertension (Ali et al., 2019; Toolabi et al., 2021). Therefore, the World Health Organization (WHO) recommends an acceptable F^- concentration of 1.50 mg/L (WHO, 1984; Mondal et al., 2014; Olaka et al., 2016; Rashid et al., 2020). The maximum permissible F^- concentration in China is 1.00 mg/L (Mao et al., 2016; Li et al., 2018; Wu et al., 2018). Groundwater is recognised as a major source of F^- ingestion (Ali et al., 2019; Yadav et al., 2021). Approximately 200 million individuals worldwide, especially those living in poor areas and developing countries, are supplied with water containing high concentrations of F^- (Currell et al., 2011; Borzi et al., 2015; Emenike et al., 2018; Thapa et al., 2018).

The Shendong mining area is one of the eight largest coalfields in the world, and the largest coalfield in the northwestern arid area of China, with annual coal production of 200 million tons (Xiao et al., 2020; Xu et al., 2021). Owing to large-scale underground coal mining, approximately 31 million tons of mine water are produced (Zhang et al., 2021). Mine water is usually used for coal production, domestic drinking water,

* Correspondence to: Xingyuan Street 58, Hebei, Shijiazhuang 050021, PR China.
E-mail addresses: haocm@ncist.edu.cn (C. Hao), sxm202109@163.com (X. Sun), 1075834936@qq.com (B. Xie), 35151765@qq.com (S. Hou).
[1] ORCID: 0000-0002-4785-2855.

https://doi.org/10.1016/j.ecoenv.2022.113496
Received 26 October 2021; Received in revised form 25 March 2022; Accepted 5 April 2022

and ecological restoration in the Shendong mining area (Zhang et al., 2011; Gu et al., 2014; Gu et al., 2021; Hao et al., 2021a, 2021b). High-F^- mine water (exceeding 1.00 mg/L) was found in several coal mines in the Shendong mining area (Hao et al., 2021a, 2021b; Zhang et al., 2021) severely threatening the water supply and ecological environment.

Many studies describe the mechanisms and geochemical processes involved in the genesis of high-F^- groundwater (Currell et al., 2011; Emenike et al., 2018; Li et al., 2018; Kumar et al., 2019). Enrichment of F^- in groundwater primarily occurs through hydrolysis of natural minerals such as fluorite, fluorspar, fluorapatite, topaz, hornblende, tourmaline, villianmite, amphiboles, mica, biotite, and muscovite (Jacks et al., 2005; Mondal et al., 2014; Dehbandi et al., 2018; Thapa et al., 2018; Wu et al., 2018). In addition, evaporation, ion exchange, and competitive effects increase F^- levels in groundwater (J. He et al., 2013; X. He et al., 2013; Olaka et al., 2016; Ali et al., 2019; Zhang et al., 2020; LaFayette et al., 2020; Hao et al., 2021a, 2021b; Toolabi et al., 2021; Yadav et al., 2021). Anthropogenic activities, such as the use of phosphate fertilisers and pesticides, aluminum smelting, glass and brick industries, coal combustion, mining activities, and semiconductor industries, also contribute a significant amount of F^- to soil and groundwater (Li et al., 2018; Rashid et al., 2018; Ali et al., 2019). Numerous hydrogeochemical environments may affect the occurrence of F^-in high-F^- groundwater, such as water with low Ca^{2+}, high Na^+, alkaline pH, and Na-HCO_3 type (J. He et al., 2013; X. He et al., 2013; Olaka et al., 2016; Abiye et al., 2018; Dehbandi et al., 2018; Knappett et al., 2018; Kumar et al., 2018).

F^- is considered a toxic element in coal (Zhang et al., 2016; Yadav et al., 2021). In the long term, abandoned and active coal mines may release F^- into groundwater (Singh et al., 2011; Zhang et al., 2016; Yadav et al., 2021). Studies have found that the F^- concentration in some mine waters have exceeded the Chinese drinking water standard (1.00 mg/L) (Yao, 2017; Gu et al., 2021; Zhang, Li et al., 2021). Although studies have been conducted on the spatial distribution and geochemical behaviour of F^- in mine water in the Shendong mining areas (Hao et al., 2021a, 2021b; Zhang et al., 2021), the sources and formation mechanisms of high-F^- mine water have received limited attention. Moreover, the impact of coal mining activities on F^- concentrations in mine water remains unclear.

Sulphur (^{34}S) and other stable isotopes ($^{18}O_{H2O}$ and D) are widely used to investigate environmental contamination problems in water, soil, and air in coal mines (Gammons et al., 2010, 2013; Wen et al., 2016; Ayadi et al., 2018; Zhou et al., 2018). The $^{34}S_{SO4}$ and $^{18}O_{SO4}$ isotopes are typically used as isotopic tracers for the source of sulfate in hydrogeological studies of mine water. In addition, since the migration of dissolved sulfate accompanies water flow, the $^{18}O_{H2O}$ and D isotopes of water can also be used as a water source tracer to identify hydrogeological processes (Samborska and Halas, 2010; Xie et al., 2017; Temovski et al., 2018; Pingping et al., 2019).

Therefore, the main objectives of this study were as follows: (1) to determine the abundance and spatial distribution of F^- in the mine water

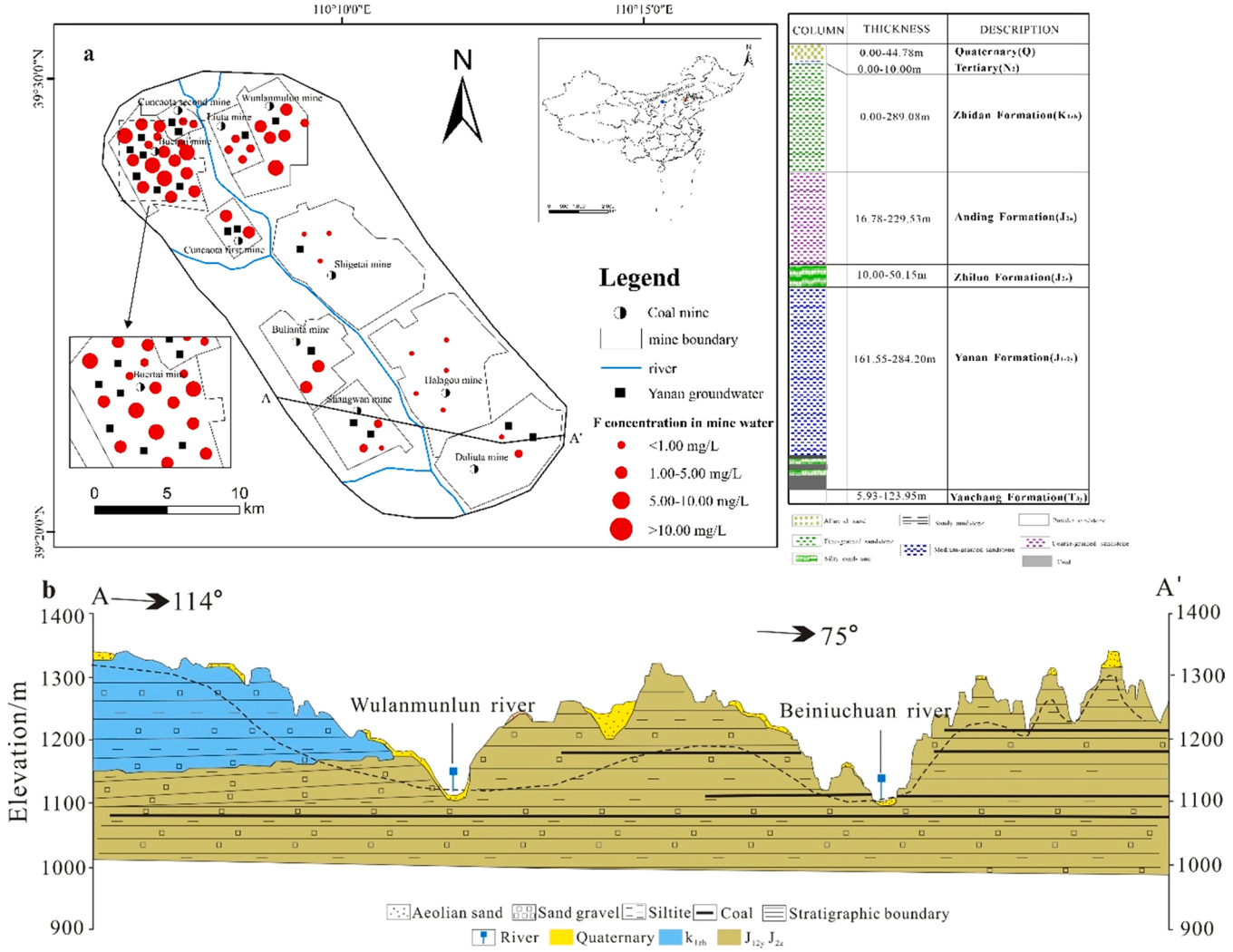

Fig. 1. a) Location of the study area and sampling sites. b) Schematic hydrogeological cross-section.

of the Shendong mining area; (2) to evaluate the hydrogeochemical behaviours and formation mechanisms that elevate F^- levels in mine water during mining activities; and (3) to study the hydrogeochemical processes of mine water at high F^- concentrations using stable isotopes ($^{34}S_{SO4}$, $^{18}O_{SO4}$,$^{18}O_{H2O}$, and D). This research will increase understanding of the hydrogeochemical processes and formation mechanisms of high-F^- mine water during mining activities. In addition, this study will aid in the policy framework for sustainable management of mine water in the region.

2. Regional geology and hydrogeology

The Shendong mining area, located at the junction of Inner Mongolia, Shanxi, and Shaanxi Provinces, is the largest coalfield in China (Fig. 1a). Its geographical coordinates are 111°04–111°11 E and 39°20–39°30 N. This mine covers an area of 3481 km^2 in a mountain range, with an altitude of 800–1385 m above sea level. The climate in the study area is a typical warm-temperate and semi-arid continental monsoon climate with an average annual rainfall, evaporation, and temperature of approximately 437.2 mm, 2065.1 mm, and 9.9 °C, respectively (Hao et al., 2021a, 2021b).

From bottom to top, the strata in the Shendong mining area mainly include the Yanchang Formation (T_{3y}) of the Upper Triassic, Yanan Formation (J_{1-2y}) of the Middle and Lower Jurassic, Zhiluo Formation (J_{2z}) and Anding Formation (J_{2a}) of the Middle Jurassic, Zhidan Formation(K_{1zh}) of the Lower Cretaceous, Tertiary(N_2), and Quaternary(Q), as shown in Fig. 1a (Xu et al., 2021; Zhang et al., 2021). Loose sediments are widely distributed in the region, and the soil type mainly includes aeolian sand and yellow loam soil, with a maximum thickness of 20–50 m.

The Shendong mining area is located on the slope belt of northern Shaanxi, which is a secondary structural unit of the Ordos Basin. The overall structure of the mining area is a monocline dipping towards the SW with a dip angle of 1–8°. Faults are rare in the mining area (Xu et al., 2021; Zhang et al., 2021). The study area has abundant coal reserves, and the recoverable coal seams include No.1^{-2}, 2^{-2}, 3^{-1}, 4^{-2}, and 5^{-2} coal seams (Xu et al., 2021). The burial depth of the coal seams varies from 60 to 400 m, and the average thickness of the coal seam is approximately 4–6 m (Hao et al., 2021a, 2021b; Zhang et al., 2021).

The yield of groundwater in this area is relatively low and occurs primarily in the porous phreatic aquifers of the Quaternary and Mesozoic pore-fissure aquifers of the clasolite (Fig. 1b). The porous phreatic aquifers of the Salawusu Formation ($Q_{3\,s}$) in the upper Pleistocene of Q_4 and pore-fissure confined aquifers of J_{1-2y} have high groundwater yield (Zhang et al., 2021). The pore-fissure confined aquifers of J_{1-2y} mainly comprise medium-coarse sandstones with extensive F^- and silicate minerals and the fractures are poorly developed (Zhang et al., 2021). These two aquifers also supply water for potable use in the Shendong mining area (Song et al., 2020; Hao et al., 2021a, 2021b; Zhang et al., 2021). The Shendong mining area produces approximately 31 million tons of mine water annually, of which only 25% is used for domestic supply and irrigation(Song et al., 2020; Gu et al., 2021; Zhang et al., 2021).

3. Materials and methods

3.1. Sample collection

In September 2020, 18 Yanan groundwater samples and 45 mine water samples were collected (Fig. 1a). Yanan groundwater samples were collected from drilling holes (depths of 35–300 m), while mine water samples were collected from fissured pipelines in the J_{1-2y} stratum and water reservoirs in underground coal mines. Before collection, the brown plastic sampling bottles were rinsed with distilled water two or three times and then rinsed with sample water two or three times. Three bottles of water were collected for each water sample: a 500 mL bottle for $\delta^{18}O_{H2O}$ and δD analysis, a 500 mL bottle for cation and anion concentration analysis, and a 5 L bottle for $\delta^{34}S_{SO4}$ and $\delta^{18}O_{SO4}$ analysis. All water samples were filtered using a 0.45 μm glass fibre membrane upon collection.

3.2. Sample analysis

The concentrations of major anions (F^-, chloride, and sulfate) and cations (calcium, magnesium, sodium, and potassium) were determined using ion chromatography (Dionex Integrion IC, Thermo Fisher, USA). The concentrations of bicarbonate and carbonate were determined using acid-base titration. The pH and total dissolved solids (TDS) values were obtained from field measurements using a portable pH meter (HANNA H18424) and portable conductivity meter (HANNA H1833), respectively.

For $\delta^{34}S_{SO4}$ and $\delta^{18}O_{SO4}$ analyses, SO_4^{2-} was precipitated as $BaSO_4$ by adding a saturated $BaCl_2$ solution with a pH value of less than 2.0, to prevent the formation of $BaCO_3$. The resultant $BaSO_4$ precipitates were purified using the diethylenetriaminepentaacetic acid (DTPA) dissolution and reprecipitation (DDARP) method (Bao, 2006; Wen et al., 2016; Li et al., 2020), rinsed several times with deionised water, and dried 12 h at 50 °C.

The isotopic results are reported as $\delta^{18}O_{H2O}$ (or δD), as defined by the following equation (Craig, 1961):

$$\delta^{18}O_{H2O}\ (\text{or } \delta D) = [(R_{sample}/R_{V-SMOW}) - 1] \times 1000\cdot$$

Where R_{sample} is the $^{18}O_{H2O}/^{16}O_{H2O}$ or $D/^1H$ ratio of the sample, and R_{V-SMOW} is $^{18}O_{H2O}/^{16}O_{H2O}$ or $D/^1H$ ratio of the standard (Gammons et al., 2010; Ayadi et al., 2018). Samples were prepared following Epstein and Mayeda (1953) for $\delta^{18}O_{H2O}$, Morrison et al. (2001) for δD, Carmody et al. (1998) for $\delta^{34}S_{SO4}$, and Kornexl et al. (1999) for $\delta^{18}O_{SO4}$.

Water isotopes δD and $\delta^{18}O_{H2O}$ were determined using a Micromass MultiPrep equipped with a dual inlet and an isotope ratio mass spectrometer (IRMS) (Institute of Hydrogeology and Geology, Chinese Academy of Geological Sciences). The analytical uncertainties of the data obtained using this instrument were ± 0.1‰ for $\delta^{18}O_{H2O}$ and ± 1‰ for δD. Moreover, $\delta^{34}S_{SO4}$ and $\delta^{18}O_{SO4}$ values were determined using a Micromass IsoPrime stable IRMS (China University of Geosciences), with analytical precisions of ± 0.2‰ and ± 0.4‰, respectively.

3.3. Analytical quality control

Experimental samples were immediately stored in ice-packed coolers after collection and shipped to a laboratory, where they were stored at 2 °C. Ten percent of the samples submitted for analysis were replicates. All analyses were performed in triplicate. Each reported value is the average of three test results, with a relative standard deviation below 10%. The detection limit of bicarbonate and carbonate analysis was 0.1 mg/L, and 0.01 mg/L for other ion analyses. The analytical precision of the ion concentrations was verified by calculating the ionic balance error. The absolute ionic balance errors of the water samples were below 5%. Twenty percent of the water samples were re-analysed, and the error between the two results was less than 10%.

3.4. Statistical analysis

The Origin 2021 software was used to perform descriptive statistical analyses and to determine correlation relationships. Piper and Gibbs diagrams were used to elucidate the hydrogeochemical facies and processes. The spatial variation of F^- was evaluated using a spatial analyst module in ArcGIS 9.3 software (ESRI, Redlands, California, USA). Descriptive data, such as the mean, range, and standard deviation, are shown in Table 1.

Table 1
Geochemistry data in different water of Shendong mining area.

Types	Na^+	K^+	Ca^{2+}	Mg^{2+}	Cl^-	SO_4^{2-}	HCO_3^-	F^-	NO_3^-	TDS	pH	δD	$\delta^{18}O_{H2O}$	$\delta^{34}S_{SO4}$	$\delta^{18}O_{SO4}$
	mg/L											‰			
Mine water (n = 45)															
Max	989.0	12.0	84.9	31.6	483.0	1114.0	1524	12.75	8.2	2967	8.5	-60	-7.6	16.8	11.3
Min	8.9	0.1	0.8	0.6	5.7	6.6	159	0.16	< 0.01	186	6.2	-86	-10.6	-0.4	1.2
Mean	459.7	4.5	25.4	8.7	266.3	208.1	708	6.10	1.6	1307	7.9	-71	-8.9	8.0	4.0
SD	274.1	3.2	25.9	8.3	144.5	254.1	379	3.76	2.1	677	0.6	7	0.8	4.0	2.4
Yanan groundwater (n = 18)															
Max	1745.0	10.0	80.5	57.6	1069.0	988.0	1345	17.60	4.4	5077	9.7	-65	-8.1	5.0	5.8
Min	10.8	0.3	0.9	0.4	5.5	3.7	131	0.01	< 0.01	195	7.0	-86	-10.6	1.3	1.9
Mean	342.1	3.2	32.6	11.9	177.3	194.6	414	3.86	1.0	1119	8.2	-71	-8.9	3.8	3.2
SD	410.9	2.3	26.7	15.2	248.4	384.0	319	4.86	1.0	1250	0.7	8	0.9	1.4	1.5

4. Results

4.1. Geochemical characterisation

The results for basic geochemical parameters such as pH, TDS, F^-, and major ions in different water samples in the Shendong mining area are shown in Table 1. Of the total, 95.56% mine water and 100% Yanan groundwater samples were from a low-alkaline environment. The TDS level exceeded the acceptable limit for drinking water of 1000 mg/L in 62.22% and 27.78% of Yanan groundwater and mine water samples, respectively (Wang et al., 2018; Hao et al., 2020a, 2020b; Chen et al., 2021). The mean TDS concentration of mine water was higher than that of Yanan groundwater.

Mine water is predominately the Na-SO_4-Cl (80.00%), Na-HCO_3 (13.33%), and Ca-HCO_3 (6.67%) type, and Yanan groundwater is the Na-HCO_3 (50.00%), Ca-HCO_3 (27.78%), and Na-SO_4-Cl (22.22%) type, as shown in Fig. 2.

4.2. F^- geochemistry

The concentration of F^- varies from 0.16 to 12.75 mg/L with a mean value of 6.10 mg/L in mine water. It was observed that 77.78% of mine water samples exceeded the national standards of China (1.00 mg/L) for drinking water (J. He et al., 2013; X. He et al., 2013; Hao et al., 2021a, 2021b). This result suggests that inhabitants who drink this water may be at risk of fluorosis.

The mapping of F^- concentrations revealed a high spatial variability within the study area (Fig. 1). Water samples from the Buetai and Cuncaota No. 2 mines in the northwest of the Shendong mining area had higher F^- concentrations than coal mines in the southeast (e.g. Halagou, Daliuta, and Shangwan mines). Compared with the Yanan groundwater, the F^- concentration was markedly increased in the mine water (Fig. 3b); the mean F^- concentration was 1.58 times of that of the Yanan groundwater. These results suggest that mining activities may contribute to increased F^- concentrations in mine water (Hao et al., 2021a, 2021b; Zhang et al., 2021). Coal mining activities may generate O_2, CO_2, and large quantities of dissolved coal and coal gangue in mine water, leading to the oxidation of pyrite in an oxidising environment and HCO_3^-

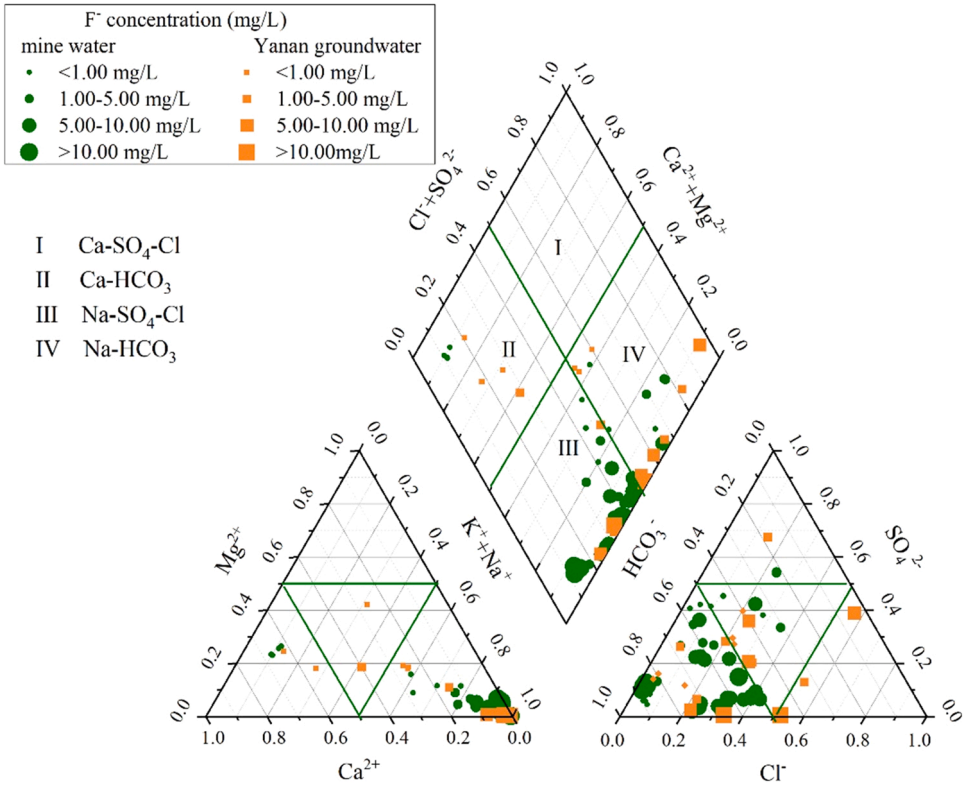

Fig. 2. Piper diagram representing groundwater facies of the study area.

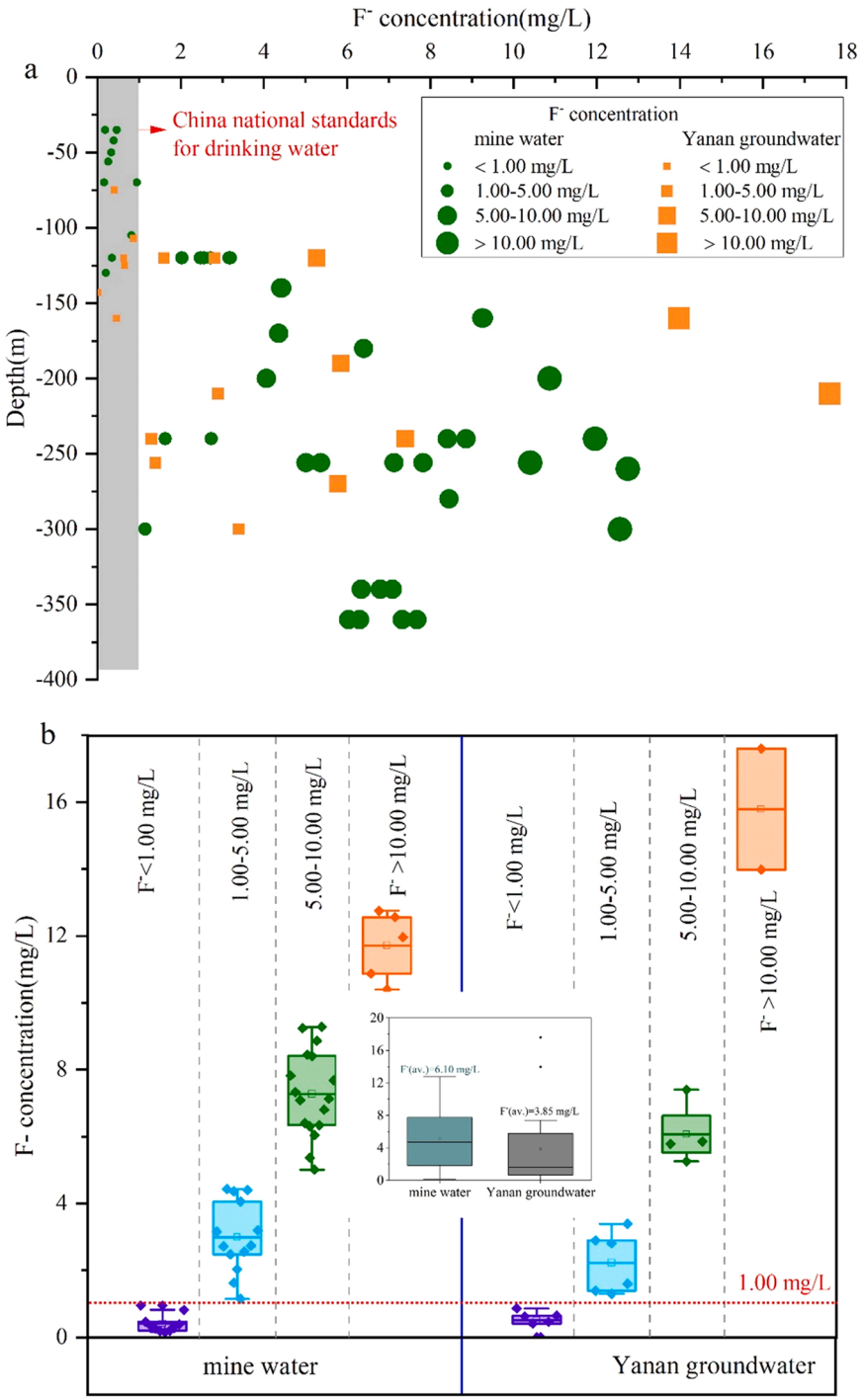

Fig. 3. The boxplots of: a) Variation in F- concentration in mine water with depth of coal seam; and b) Comparison of F^- distribution in different water types in the Shendong mining area.

enrichment (Zhang et al., 2021). Therefore, the mean SO_4^{2-} and HCO_3^- concentrations were higher in the mine water enrichment than in the Yanan groundwater (Table 1).

Based on the Chinese national standards for drinking water and concentration risk of fluorosis, the mine water samples were divided into four groups: < 1.00 mg/L (low-F^- mine water), 1.00–5.00 mg/L, 5.00–10.00 mg/L, and > 10.00 mg/L. Where the F^- concentration is higher than 1.00 mg/L, this is referred to as high-F^- mine water. Most of the high-F^- mine water samples also contained greater than 1000 mg/L TDS (Table 1), indicating more complex water-rock interactions in high-F^- mine water (Li et al., 2016; Salcedo Sánchez et al., 2017; Palma et al., 2019).

There was a clear relationship between the F^- concentration and depth (Fig. 3a). High-F^- mine water samples from fissured pipelines in the J_{1-2y} stratum and water reservoirs in underground coal mines were collected at a depth of 150–350 m. In contrast, low-F^- mine water samples were collected from a depth of 50–150 m, where the groundwater flow is generally slow owing to a low hydraulic gradient (Zhang et al., 2021). The slow flow and a low hydraulic gradient support F^- enrichment in mine water (J. He et al., 2013; X. He et al., 2013). Mine water samples with F^- concentrations above 10.00 mg/L were of the Na-SO_4-Cl type of water. The mine water samples with F^- concentrations

between 1.00 mg/L and 5.00 mg/L and between 5.00 mg/L and 10.00 mg/L were of the Na-SO_4-Cl and Na-HCO_3 water type, respectively, with the Na-HCO_3 water type accounting for a relatively larger proportion (77.78%). In contrast, low-F^- mine water samples (F^- concentration below 1.00 mg/L) were Ca-HCO_3, Na-HCO_3, and Na-SO_4-Cl types (Fig. 2).

4.3. Hydrogen and oxygen isotopic characteristics

As shown in Table 1, the $\delta^{18}O_{H2O}$ and δD content of the mine water samples ranged from − 10.6‰ to − 7.6‰ [mean − 8.9 ± 0.8‰, standard mean ocean water (SMOW)], and from − 86‰ to − 60‰ (mean −71 ± 7‰, SMOW), respectively. As shown in Fig.S1, mine water samples lie below and to the right of the local meteoric water line (LMWL: $\delta D = 6.8 \times \delta^{18}O_{H2O}$-0.4, Liu., 2018 and Guo et al., 2021, from139 groups of isotopic statistics data for precipitation in the Ordos Basin) and the global meteoric water line (GMWL: $\delta D = 8.0 \times \delta^{18}O_{H2O} + 10.0$, Craig. H. 1961). Almost 94.12% of mine water samples appeared below the LMWL, probably owing to evaporation effects (Gammons et al., 2006; Wen et al., 2016; Hao et al., 2019). A total of 87.50% of Yanan groundwater and 88.89% of mine water samples were plotted together with similar $\delta^{18}O_{H2O}$ and δD values, indicating that the Yanan groundwater and mine water samples have the same water source (Yan et al., 2020; Hao et al., 2021a, 2021b; Zhang et al., 2021). The results confirm that the mine water originates from the Yanan groundwater. In addition, the Yanan groundwater samples plotted in the $\delta^{18}O_{H2O}$ and δD diagrams between − 86‰ and − 65‰ for $\delta^{18}O_{H2O}$ and between − 10.6‰ and − 8.1‰ for δD in the local recharge of the precipitation value range ($\delta^{18}O_{H2O}$: −153.4‰ ~ −5.1‰ and δD: −13.6‰ ~ −4.8‰ from Liu, 2008 and Guo et al., 2021) and suggest that the Yanan groundwater is of meteoric origin. The δD and $\delta^{18}O_{H2O}$ values of high-F^- mine water were relatively poorer than those in low-F^- mine water, indicating high-F^- mine water samples have more intense water-rock interactions (e.g. the dissolution of F-bearing minerals) (Guo et al., 2021).

The mine water samples fell in the Na-SO_4-Cl type (80.00% of the total samples) and Na-HCO_3 type (13.33% of the total samples) (Fig. 2). In contrast, 50.00% and 27.78% of the Yanan groundwater samples were the Na-SO_4-Cl type and Na-HCO_3 type, respectively. From the plot, most mine water samples transformed gradually from the Na-HCO_3 type to the Na-SO_4-Cl type with increasing F^- concentration. Moreover, the chemistry of mine water is similar to that of Yanan groundwater (Table 1) and combined with local hydrogeological conditions indicate that Yanan groundwater is the main recharge source of high-F^- mine water (Guo et al., 2021; Hao et al., 2021a, 2021b). It should be with regret that the recharge source for mine water is merely discussed with Yanan water, and other recharge sources (i.e. precipitation) were not considered in this study.

5. Discussion

5.1. Dissolution/precipitation process

The plot of water samples on the Gibbs diagram (Fig.S2a), which is used to determine the mechanisms that control water geochemistry, revealed that water geochemistry is influenced by precipitation and mineral dissolution (Gibbs, 1970; Dehbandi et al., 2018; Ali et al., 2019). Usually, in Gibb's diagram, the evaporation/precipitation effect has a TDS value above 10,000 mg/L and a $Na^+/(Na^+ + Ca^{2+})$ value of approximately 1.0. The rain dissolution dominance field, located at the lower right of the diagram, has low TDS and $Na^+/(Na^+ + Ca^{2+})$.

Results indicate that the geochemistry of mine water in the Shendong mining area is controlled by rock weathering and evaporation/precipitation processes. With an increase in F^- concentration above 1.00 mg/L concentration, the mine water samples moved horizontally to the right in the diagram along the rock weathering zone. $Na^+/(Na^+ + Ca^{2+})$ values increased and tended to reach 1.0, and TDS values also increased, indicating that high-F^- mine water has higher intensity water-rock interactions (Rashid et al., 2018; Thapa et al., 2018; Hao et al., 2021a, 2021b). Generally, mine water contains large quantities of dissolved coal and coal gangue from mining activities, thereby enhancing the water-rock interaction process.

Yanan groundwater samples have similar values of $Na^+/(Na^+ + Ca^{2+})$ and TDS as the mine water samples (Fig.S2a), indicating similar rock weathering and evaporation/precipitation processes. This suggests that rock weathering and evaporation/precipitation processes were not the major factors for the elevation of F^- in mine water.

Previous studies found extensive F^- minerals such as fluorite (CaF_2), phosphorite ($Ca_5(PO_4)_3F$), and diorite ($NaCa_2(Mg,Fe,Al)_5(Al,Si)_8O_{22}F_2$) in the J_{1-2y} stratum of the Shendong mining area (Zhao and Wei, 2020; Duan et al., 2021), comprising predominately medium-grained and silty sandstones. The average F^- content in the coals of the Shendong mining area is 803.5 mg/kg, with an average soluble F content of 4.10–9.45% (Zhao and Wei, 2020).

The common weathering reaction for fluorite (CaF_2) is simple dissolution, resulting in a Ca^{2+}: F^- equivalence ratio of 1:2, as shown in Fig. S2b and Eq. (1):

$$CaF_2 + H_2O + CO_2(g) \rightarrow CaCO_3 + 2\,F^- + 2\,H^+ \quad (1)$$

In the diorite weathering reaction, the equivalence ratio of Ca^{2+}: F^- is maintained at 1:1, as shown in Fig.S2b and Eq. (2).

$$NaCa_2(Mg,Fe,Al)_5\,(Al,Si)_8O_{22}F_2 + 2OH^- \rightarrow NaCa_2(Mg,Fe,Al)_5\,(Al,Si)_8O_{22}(OH)_2 + 2\,F^- \quad (2)$$

In the pure phosphorite dissolving reaction, the equivalence ratio of Ca^{2+}: F^- was maintained at 5:1, as shown in Fig.S2b and Eq. (3):

$$Ca_5(PO_4)_3F + OH^- \rightarrow Ca_5(PO_4)_3(OH) + F^- \quad (3)$$

As shown in Fig.S2b, Yanan water samples were distributed from the phosphorite dissolution line to the diorite dissolution line, accompanied by increased F^-concentration from below 1.00 mg/L to above 10.00 mg/L. This provides strong evidence that the dissolution of fluorite and diorite minerals is the key factor that increases the F^- concentration in the Yanan groundwater.

Similar to the Yanan groundwater, the mine water samples were scattered from the phosphorite dissolution line to the diorite dissolution line, suggesting that dissolution of F-bearing minerals had a minor influence on the elevated F^- concentration in mine water.

5.2. Ion exchange process

Generally, two chloroalkaline ion exchange (CAI) indices are used to evaluate the influence of ion exchange and reverse ion exchange on the geochemical composition of groundwater (Schoeller, 1965; J. He et al., 2013; X. He et al., 2013; Kaur et al., 2019). Schoeller (1965) defined two chloroalkaline ion-exchange indices as follows:

$$CAI\ 1 = [Cl\text{-}(Na + k)]/Cl \quad (4)$$

$$CAI\ 2 = [Cl\text{-}(Na + k)]/(HCO_3 + CO_3 + NO_3) \quad (5)$$

A positive CAI indicates that Na^+ and K^+ present in water were exchanged with Ca^{2+} and Mg^{2+} during contact with the aquifer material, representing the reverse ion exchange process, whereas a negative CAI implies that Ca^{2+} and Mg^{2+} in groundwater were exchanged with K^+ and Na^+, representing ion exchange. In addition, the larger the absolute values of CAI 1 and CAI 2, the stronger the ion-exchange interaction (Wang et al., 2015; Kaur et al., 2019). A CAI value of 0 indicates that ion exchange did not occur during groundwater formation. In Fig. 4a, 100% of mine water and 88.89% of Yanan groundwater samples show negative CAI 1 and CAI 2 values, implying that Ca^{2+} and Mg^{2+} in the Yanan groundwater and mine water were exchanged with Na^+ and

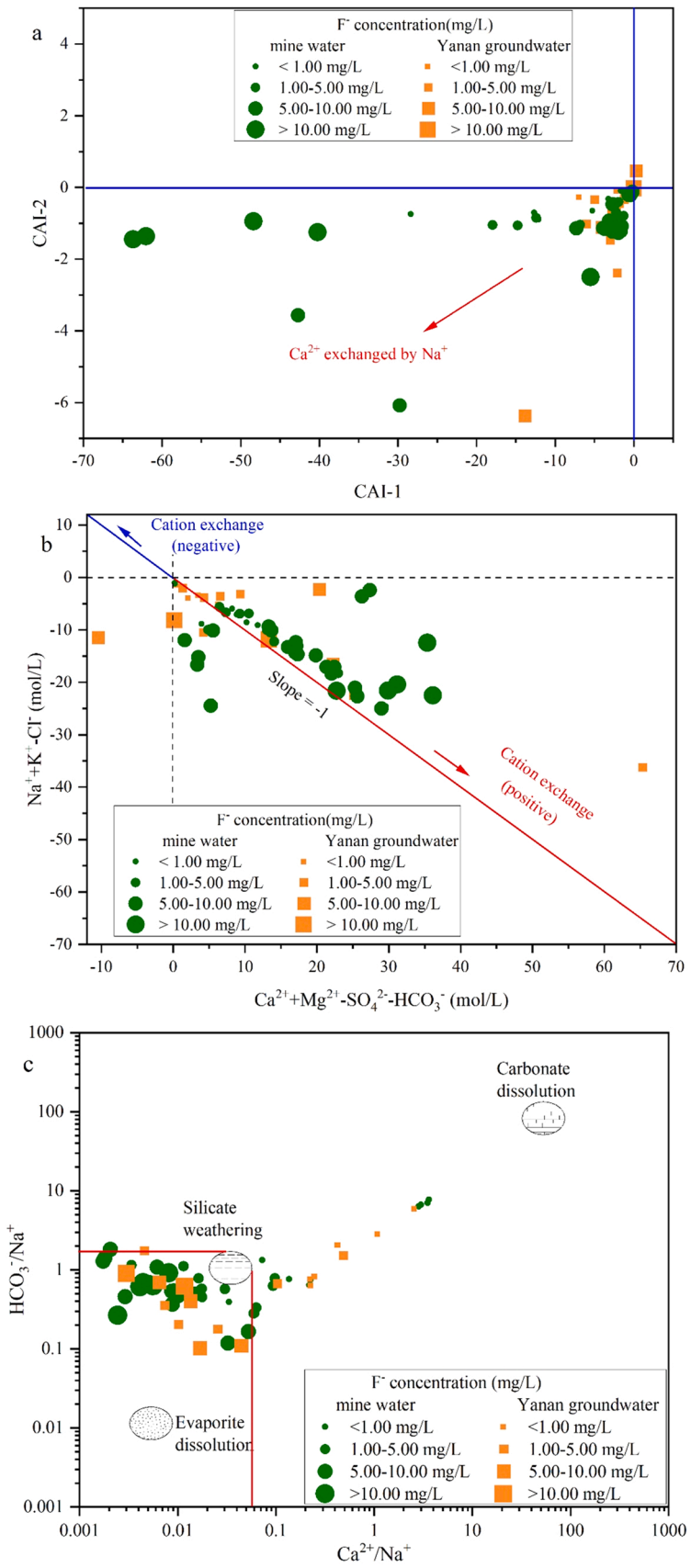

Fig. 4. Plots of: a) CAI 1 versus CAI 2; b) (Ca^{2+} + Mg^{2+}-SO_4^{2-} - HCO_3^-) versus (Na^+ + K^+ - Cl-), and c) HCO_3^-/Na^+ versus Ca^{2+}/Na^+ of the Shendong Mine water samples.

K^+ in the surrounding aquifer material. Firstly, the increased Na^+ and K^+ concentrations reduce the repulsive potential between the positively charged hydroxide surface and the negatively charged anions at alkaline pH, facilitating F^- desorption into mine water (Li et al., 2015). Secondly, lower Ca^{2+} conditions favoured fluorite dissolution, which increased the concentration of F^- in the mine water. The more rapid the decrease in Ca^{2+} concentration, the greater the increase in F^- concentration (LaFayette et al., 2020; Hao et al., 2021a, 2021b). Moreover, the CAI value of mine water was higher than that of the Yanan groundwater, indicating that ion-exchange interactions were more dominant in mine water. Thus, the cation exchange process primarily increases the F^- concentration in mine water.

Of the mine water samples, 82.22% were saturated or over-saturated with calcite and dolomite as shown in Fig.S3a–c. The saturation of calcite and dolomite reduces the Ca^{2+} and Mg^{2+} concentrations of mine water and accelerates the dissolution of fluorite, increasing the F^- concentration. The saturation indices (SI) of the halite are less than 0 (Fig. S3d), indicating that the halite was unsaturated and promoted more Na^+ and K^+ enrichment in mine water. The F^- concentration is positively correlated with the saturation coefficient SI of fluorite (Fig.S3e). The higher the F^- concentration, the stronger the SI of fluorite, which indicates that the dissolution of F-bearing minerals (such as fluorite) contributes significantly to the F^- concentration in mine water (Wang et al., 2015; Kaur et al., 2019). For gypsum, the SI is negative (Fig.S3f), indicating that the gypsum mineral is under-saturated and dissolution will occur. $(Ca^{2+} + Mg^{2+} - HCO_3^- - SO_4^{2-})$ versus $(Na^+ + K^+ - Cl^-)$ was

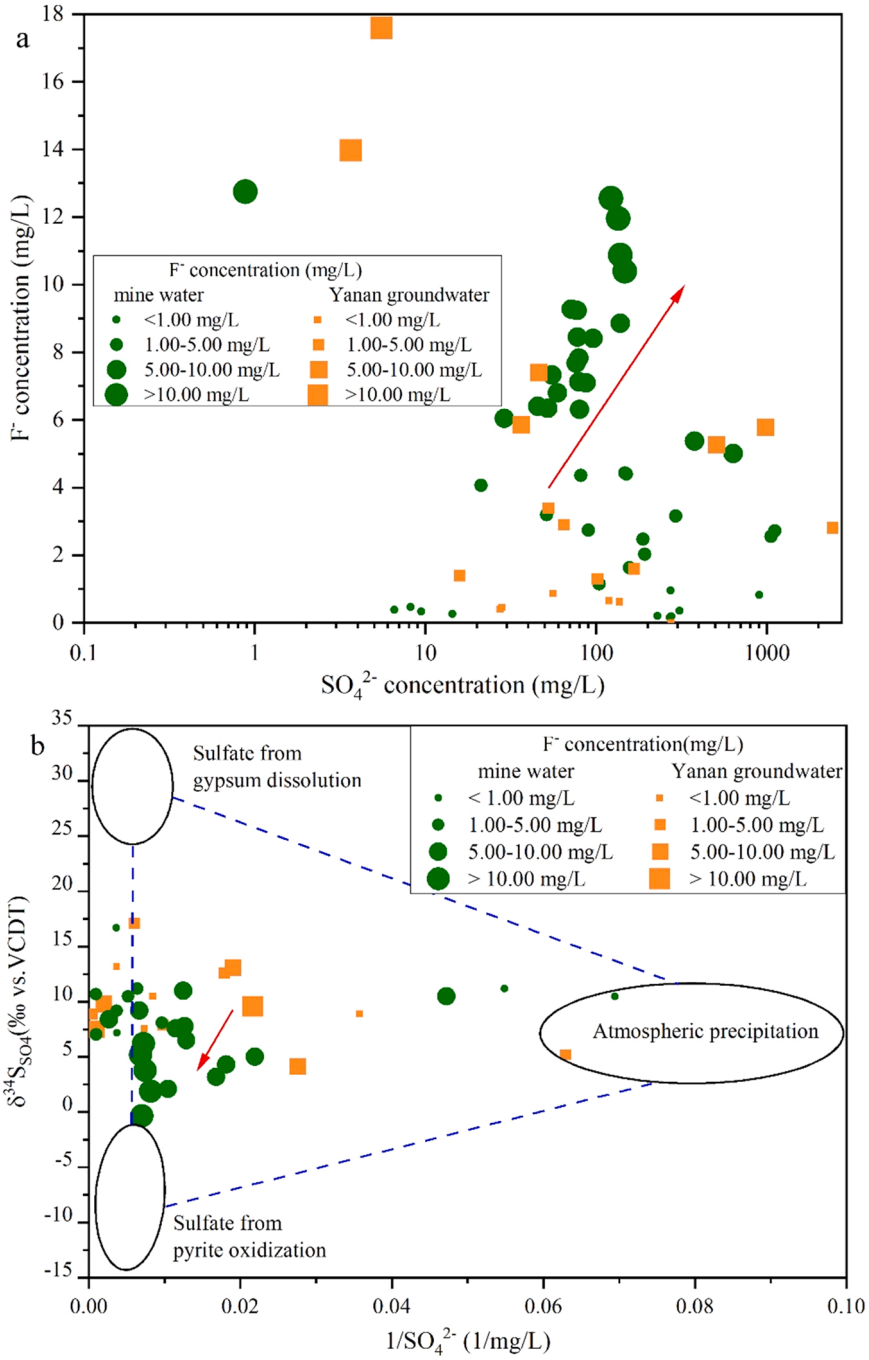

Fig. 5. The plots of: a) SO_4^{2-} versus the F^- concentration; and b) Relationship between $\delta^{34}S$ (SO_4^{2-}) and the inverse of SO_4^{2-} for samples collected in the Shendong mining area.

identified as further evidence of cation exchange (Fig. 4b). When the relationship between the two parameters is linear, with a slope of − 1, cation exchange is a driving process(Kim et al., 2004; Gao et al., 2009; Kaur et al., 2019).

As shown in Figs. 4b, 50.00% of the Yanan groundwater and 71.11% of the mine water samples were distributed around a line with a slope of − 1, further indicating that cation exchange is the main potential source of Na^+ in the groundwater. Owing to the positive cation exchange reaction, Na^+ from the surrounding aquifer material is gradually released into the mine water, while the Ca^{2+} concentration gradually decreases. The absolute values of (Ca^{2+} + Mg^{2+}–HCO_3^-—SO_4^{2-}) and (Na^++K^+–Cl^-) in the mine water were greater than those in the Yanan groundwater, indicating that more Ca^{2+} was exchanged with Na^+ and K^+. This could strengthen the free migration ability of F^- in mine water (Yan et al., 2020). Fig. 4c shows that high-F^- mine water samples are located around the silicate weathering field, indicating that the dominant mineral in the weathering process of mine water is silicate. Moreover, (Na^+ + K^+) and HCO_3^- display a positive correlation with F^- in mine water ($R^2 = 0.57$ in Fig.S2d and $R^2 = 0.43$ in Fig.S5). This suggests that weathering reactions of silicate rocks (i.e.muscovite and biotites) could lead to simultaneous F^-, Na^+, and K^+ enrichment when excess CO_2 is released into the mine water through mining activities (Rashid et al., 2020; Dehbandi et al., 2018; Li et al., 2018). The process can be described by Eqs. (6) and (7), as follows:

$$KAl_3Si_3O_{10}(OH\text{-}F)_2 + CO_2 + 2.5H_2O \rightarrow 1.5Al_2Si_2O_5(OH)_4 + K^+ + 2F^- + HCO_3^- \quad (6)$$

$$NaMg_3AlSi_3O_{10}(OH\text{-}F)_2 + 7CO_2 + 7.5H_2O \rightarrow 0.5Al_2SiO_5(OH)_4 + Na^+ + 3Mg^{2+} + 2F^- + 2H_4SiO_4 + 7HCO_3^- \quad (7)$$

High concentrations of sulfate in mine water have positive relationships with F^- (Fig. 5a), suggesting a significant effect of salinity on F^- levels (Emenike et al., 2018; Li et al., 2018). Sulphur and oxygen isotopic geochemistry are useful in tracing and interpreting the formation of sulfate (Sun et al., 2017; Nariyan et al., 2018; Zhou et al., 2018; Kim et al., 2019). According to the literature, there are several different sources of sulfate in mine water, including atmosphere precipitation, sulfate mineral dissolution (i.e.gypsum), bacterial sulfate reduction, and oxidization of sulfate minerals(i.e.pyrite) (Samborska and Halas, 2010; Gammons et al., 2013; Zhou et al., 2018; Kim et al., 2019). The $\delta^{34}S_{SO4}$ in mine water is stable in the range of − 0.4–16.8‰ (Table 1) and lies above the approximate range (slopes of lines from Gammons et al., 2013) of bacterial sulfate reduction during kinetic isotopic fractionation (Fig. S4a). There is little evidence for the influence of bacterial sulfate reduction on the isotopic composition of dissolved SO_4^{2-}(Zhou et al., 2018).

As shown in Fig. 5b, the $\delta^{34}S_{SO4}$ in the mine water samples falls between the pyrite oxidation field and gypsum dissolution field, but far from the atmospheric precipitation field, suggesting that pyrite oxidation and gypsum dissolution are the main sources of SO_4^{2-} enrichment in mine water. When the F^- concentration is 5.00–10.00 mg/L and above 10.00 mg/L, the mine water samples scatter significantly deviate from the gypsum dissolution line (Fig.S4c), implying the influence of pyrite oxidisation and higher SO_4^{2-} mean concentrations compared with Yanan groundwater samples (Table 1).

The $\delta^{34}S_{SO4}$ value in mine water changes slightly with depth (Fig. S4b), which indicates that the water is oxide water (Zhou et al., 2018). In this study, the total sulphur content in the coals of the Shendong mining area is generally 0.2–0.8% (mean 0.4%), mainly comprising pyrite sulphur (Zhang et al., 2021). When O_2 enters the coal seam and mine water during coal mining activities, pyrite in the coal seam generates SO_4^{2-}, owing to oxidation potential (Kefeni et al., 2017; Ghosh et al., 2018; Kim et al., 2019). In addition,97.78% of mine water had a weakly alkaline pH, which was influenced by carbonates that provided sufficient pH buffering ability (Gammons et al., 2013; Wen et al., 2016). The mean HCO_3^- concentration in mine water was significantly higher than in the Yanan groundwater (Table 1), pointing to the involvement of carbonate minerals in the geochemical processes.

The average value of $\delta^{34}S_{SO4}$ in mine water was 8.0‰, which is much lower than that of the Yanan groundwater (Table 1), suggesting a different source of SO_4^{2-}. Compared with the Yanan groundwater samples, the $\delta^{34}S_{SO4}$ value of mine water samples shifts to the pyrite oxidisation field (especially for F^- concentration between 5.00 mg/L and 10.00 mg/L and above 10.00 mg/L). Thus, pyrite oxidation played a more important role as a source of SO_4^{2-}, as the mean F^- concentration in the mine water was markedly higher than that in the Yanan groundwater (Fig. 3b and Table 1).

The process may be described by Eqs. (8)-(10) as follows:

$$FeS_2 + 7/2O_2 + H_2O \rightarrow Fe^{2+} + 2SO_4^{2-} + 2H^+ \quad (8)$$

$$Ca^{2+} + SO_4^{2-} + 2H_2O \rightarrow CaSO_4{\cdot}2H_2O \quad (9)$$

$$CaSO_4{\cdot}2H_2O + 2F^- \rightarrow CaF_2 + SO_4^{2-} + 2H_2O \quad (10)$$

The solubility of calcium fluoride ($Ksp[CaF_2] = 5.3 \times 10^{-9}$) is considerably lower than that of calcium sulfate ($Ksp[CaSO_4{\bullet}2\,H_2O] = 3.1 \times 10^{-5}$) (Shao et al., 2021). Thus, excessive sulfate inhibits the precipitation of calcium sulfate. Based on Eqs. (8) and (10), the oxidative dissolution of FeS_2 generates SO_4^{2-}, and increasing SO_4^{2-}concentrations will cause a leftward shift in the equilibrium [Eq. (10)] leading to an increase in F^- concentration in mine water. The result confirms that the SI mean values of fluorite in mine water (mean:−0.86) were slightly stronger than that in Yanan groundwater(mean:−1.01) (Fig.S3e). Therefore, the elevated SO_4^{2-}concentrations will help to reduce the concentration of Ca^{2+} and to lower down the SI value of fluorite, resulting in higher levels of F^-in mine water compared with Yanan groundwater (Gao et al., 2007; Li et al., 2018).

5.3. Competitive effect

In an alkaline environment, HCO_3^- and OH^- in groundwater compete with clay minerals for F^- anions (Guo et al., 2012; Ali et al., 2019). The F^- concentration in the mine water showed an increasing trend with HCO_3^-, as shown in Fig. S5. F^- is slightly positively related to pH (from 7.5 to 8.5), as shown in Fig S2c, which indicates that alkaline environmental conditions can elevate the F^-concentration in mine water. Samples with F^- concentrations between 5.00 mg/L and 10.00 mg/L and above 10.00 mg/L samples fall near the pH = 8.33 line, indicating higher HCO_3^- content. In the mine water, the HCO_3^- concentration is higher than that of Yanan groundwater due to higher CO_2 levels. This suggests that the competitive effect increased in mine water and significantly elevated the F^- concentration (Fig. S5). Alkaline environmental conditions increase the positive charge of sorbents on mineral surfaces, and F^-desorption occurs (Guo et al., 2012; Li et al., 2018). However, oxy-hydroxides of Al, Fe, and clay minerals may act as F^- adsorbents. The formation of F on mineral surfaces is vital to groundwater F^- enrichment during the competitive effect process. Therefore, further studies are required to determine the form of F release in mine water. Excess OH^- can accelerate the weathering of F-bearing minerals such as diorite or phosphorite, enhancing F^- solubility in mine water (Ali et al., 2019).

5.4. Agricultural and domestic activities

High levels of nitrate (NO_3^-) are considered indicative of agricultural activities, such as application of fertilisers (i.e. urea) or generation of animal wastes (i.e. manure), and domestic activities (Sharma and Subramanian, 2008; Ali et al., 2019). The pollution limit for NO_3^- is 5 mg/L (Heaton, 1986; Li et al., 2018; Hao et al., 2021a, 2021b). As shown in Fig. S6b, for the mine water samples with F^- concentration between 5.00 mg/L and 10.00 mg/L and above 10.00 mg/L, the correlation between NO_3^- and F^- is insignificant, which indicates agriculture and domestic activities are not key factors for F^- enrichment in mine water.

Untreated irrigation effluent, synthetic fertilisers, and runoff from surrounding agricultural fields can infiltrate the mine water through goaf fissures (Ali et al., 2018; Li et al., 2021; Su et al., 2021). The enrichment of F^- in mine water is facilitated by the direct input of F^-. Gaseous and particulate F^- emissions from coal dust are an important source of atmospheric F pollution in the study area (Zhong et al., 2017; Yadav et al., 2021; Zango et al., 2021). Meanwhile, F in mine water originates from domestic sewage and waste. However, the similarly weak correlation between the values of NO_3^- and Cl^- and between NO_3^- and F^- concentration in mine water and Yanan mine water indicates that agriculture and domestic activities had minimal impact on the further enrichment of F^- in mine water (Ali et al., 2019; Hao et al., 2021a, 2021b).

5.5. Formation mechanisms that increase F^- levels in mine water

A schematic diagram demonstrating F^- enrichment in Shendong mine water is shown in Fig. 6. The F^- from Yanan groundwater is initially mobilised through coal mining activities. When O_2, CO_2, and large quantities of coal and coal gangue are dissolved in mine water, a cation exchange process, such as silicate weathering, occurs and induces a decrease in Ca^{2+} concentration, leading to the dominance of Na^+ and K^+ ions in the mine water. The reduced Ca^{2+} concentration promotes the leaching of F^- from F-bearing minerals (i.e. fluorite, phosphorite, and diorite) into the mine water. Meanwhile, the increased Na^+ and K^+ concentrations reduce the repulsive potential between the positively charged hydroxide surface and the negatively charged anions at alkaline pH, facilitating further F^- desorption into the mine water.

The oxidation of pyrite in a coal seam under an oxidising environment leads to SO_4^{2-} concentration enrichment in mine water during mining activities. Increasing SO_4^{2-}concentrations prevent the precipitation of CaF_2, leading to higher F^- solubility in mine water than in Yanan groundwater. Furthermore, an increase in HCO_3^- concentration also contributes to the elevated F^- concentration. Firstly, the presence of HCO_3^- can reduce the available adsorption sites of the sorbents, resulting in the release of exchangeable F^-. Secondly, the presence of HCO_3^- could promote the weathering dissolution of F-bearing minerals, leading to F^- enrichment in mine water. As such, agriculture, and domestic activities do not influence the F^- concentration in mine water mining activities.

6. Conclusions

This study was carried out to investigate mine water, and our findings revealed the spatial distribution, hydrogeochemical behaviours, and formation mechanisms of F^- concentrations in mine water during mining activities.

In this study, the concentration of F^- varies from 0.16 to 12.75 mg/L with a mean value of 6.10 mg/L in mine water, and 77.78% of the mine water samples had a concentration that exceeded that of the national standards of China (1.00 mg/L) for drinking water. In the Shendong mining area, water samples from coal mines in the northwest had higher F^- concentrations than those from other coal mines in the southeast. With similar $\delta^{18}O_{H2O}$ and δD values, the mine water originated from the Yanan groundwater, however, the F^- concentration increased further in mine water, with the mean F^- concentration being 1.58 times of that in Yanan groundwater.

O_2, CO_2, and large quantities of coal and coal gangue are mixed in the mine water during mining activities. Thus, cation exchange and competitive effects seem to be the dominant factors controlling the further increase of F^- concentration in mine water. Pyrite oxidation generates more SO_4^{2-}, which causes more Ca^{2+} decrease in mine water, leading to a greater increase in the F^- concentration than in the Yanan groundwater.

Furthermore, high HCO_3^-, Na^+, and K^+ concentrations reduce the available adsorption sites of exchangeable F^- at alkaline pH and promote the weathering dissolution of F-bearing minerals, leading to more F^- release into mine water. Thus, the weathering of F-bearing minerals, agriculture, and domestic activities do not play a significant role in controlling the secondary enrichment of F- concentration in mine water.

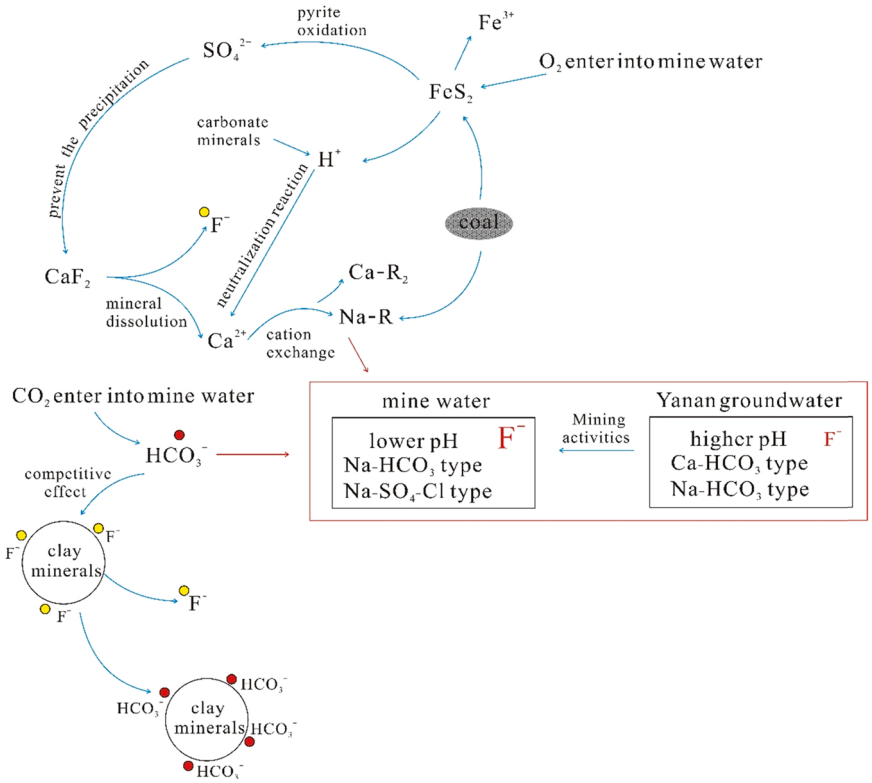

Fig. 6. Mechanism of formation of high-F^- mine water.

This research will aid in improving the understanding of the geochemical behaviour of F^- in mine water during mining activities and provide useful insights for the sustainable management of mine water resources and the safety of drinking water within the study area.

CRediT authorship contribution statement

Chunming Hao: Conceptualization, Methodology, Writing – original draft. **Ximeng Sun:** Data curation, Visualization, Investigation. **Bing Xie:** Software, Investigation. **Shuanglin Hou:** Supervision, Writing – review & editing.

Declaration of Competing Interest

The authors declare no conflict of interest.

Acknowledgements

This work was supported by the Natural Science Foundation of Hebei Province (D2021508004), the Open Fund of State Key Laboratory of Groundwater Protection and Utilization by Coal Mining (grant number SHJT-17-42.17), and the ecological restoration project in the Lengshuijiang Antimony Mine Area (grant LCG2020009).

Appendix A. Supporting information

Supplementary data associated with this article can be found in the online version at doi:10.1016/j.ecoenv.2022.113496.

References

Abiye, T., Bybee, G., Leshomo, J., 2018. Fluoride concentrations in the arid Namaqualand and the Waterberg groundwater, South Africa: understanding the controls of mobilization through hydrogeochemical and environmental isotopic approaches. Groundw. Sustain. Dev. 6, 112–120.
Aghapour, S., Bina, B., Tarrahi, M.J., Amiri, F., Ebrahimi, A., 2018. Distribution and health risk assessment of natural fluoride of drinking groundwater resources of Isfahan, Iran, using GIS. Environ. Monit. Assess. 190, 137.
Ali, S., Shekhar, S., Bhattacharya, P., Verma, G., Chandrasekhar, T., Chandrashekhar, A. K., 2018. Elevated fluoride in groundwater of Siwani Block, Western Haryana, India: a potential concern for sustainable water supplies for drinking and irrigation. Groundw. Sustain. Dev. 7, 410–420.
Ali, W., Aslam, M.W., Junaid, M., Ali, K., Guo, Y., Rasool, A., Zhang, H., 2019. Elucidating various geochemical mechanisms drive fluoride contamination in unconfined aquifers along the major rivers in Sindh and Punjab, Pakistan. Environ. Pollut. 249, 535–549.
Ayadi, Y., Mokadem, N., Besser, H., Khelifi, F., Harabi, S., Hamad, A., Boyce, A., Laouar, R., Hamed, Y., 2018. Hydrochemistry and stable isotopes (δ 18 O and δ 2H) tools applied to the study of karst aquifers in southern mediterranean basin (Teboursouk area, NW Tunisia). J. Afr. Earth Sci. 137, 208–217.
Bao, H., 2006. Purifying barite for oxygen isotope measurement by dissolution and reprecipitation in a chelating solution. Anal. Chem. 78, 304–309.
Battaleb, L., Moore, F., Malde, M.K., Jacks, G., 2013. Fluoride in groundwater, dates and wheat: Estimated exposure dose in the population of Bushehr, Iran. J. Food Compos. Anal. 29, 94–99.
Borzi, G.E., Garcia, L., Carol, E.S., 2015. Geochemical processes regulating F-, as and NO3- content in the groundwater of a sector of the Pampean Region, Argentina. Sci. Total Environ. 530–531, 154–162.
Carmody, R.W., Plummer, L.N., Busenberg, E., Coplen, T.B., 1998. Methods for collection of dissolved sulfate and sulfide and analysis of their sulfur isotopic composition. US Geol. Surv. 97–234.
Chen, J., Gao, Y., Qian, H., Ren, W., Qu, W., 2021. Hydrogeochemical evidence for fluoride behavior in groundwater and the associated risk to human health for a large irrigation plain in the Yellow River Basin. Sci. Total Environ., 149428
Craig, H., 1961. Isotopic variations in meteoric waters. Science 133, 1702–1703.
Currell, M., Cartwright, I., Raveggi, M., Han, D., 2011. Controls on elevated fluoride and arsenic concentrations in groundwater from the Yuncheng Basin, China. Appl. Geochem. 26, 540–552.
Dehbandi, R., Moore, F., Keshavarzi, B., 2018. Geochemical sources, hydrogeochemical behavior, and health risk assessment of fluoride in an endemic fluorosis area, central Iran. Chemosphere 193, 763–776.
Deng, Y., Nordstrom, D.K., McCleskey, R.B., 2011. Fluoride geochemistry of thermal waters in Yellowstone National Park: I. Aqueous fluoride speciation. Geochim. Cosmochim. Acta 75, 4476–4489.
Duan, L., Wang, X., Sun, Y., 2021. Occurrence characteristics and ecological risk assessment of fluorine in coal gangue. Coal Convers. 44, 1–10.
Emenike, C.P., Tenebe, I.T., Jarvis, P., 2018. Fluoride contamination in groundwater sources in Southwestern Nigeria: assessment using multivariate statistical approach and human health risk. Ecotoxicol. Environ. Saf. 156, 391–402.
Epstein, S., Mayeda, T., 1953. Variation of O-18 content of waters from natural sources. Geochim. Cosmochim. Acta 4, 213–224.
Gammons, C.H., Poulson, S.R., Pellicori, D.A., Reed, P.J., Roesler, A.J., Petrescu, E.M., 2006. The hydrogen and oxygen isotopic composition of precipitation, evaporated mine water, and river water in Montana, USA. J. Hydrol. 328, 319–330.
Gammons, C.H., Duaime, T.E., Parker, S.R., Poulson, S.R., Kennelly, P., 2010. Geochemistry and stable isotope investigation of acid mine drainage associated with abandoned coal mines in central Montana, USA. Chem. Geol. 269, 100–112.
Gammons, C.H., Brown, A., Poulson, S.R., Henderson, T.H., 2013. Using stable isotopes (S, O) of sulfate to track local contamination of the Madison karst aquifer, Montana, from abandoned coal mine drainage. Appl. Geochem. 31, 228–238.
Gao, X., Wang, Y., Li, Y., Guo, Q., 2007. Enrichment of fluoride in groundwater under the impact of saline water intrusion at the salt lake area of Yuncheng basin, northern China. Environ. Geol. 53, 795–803.
Ghosh, S., Golding, S.D., Varma, A.K., Baublys, K.A., 2018. Stable isotopic composition of coal bed gas and associated formation water samples from Raniganj Basin, West Bengal, India. Int. J. Coal Geol. 191, 1–6.
Gibbs, R., 1970. Mechanisms controlling world's water chemistry. Science 170, 1088–1090.
Goodarzi, F., Mahvi, A.H., Hosseini, M., 2017. Prevalence of dental caries and fluoride concentration of drinking water: a systematic review. Dent. Res. J. 14, 163–168.
Gu, D., Li, J., Cao, Z., 2021. Technology and engineering development strategy of water protection and utilization of coal mine in China. J. China Coal Soc.
Guo, H., Zhang, Y., Xing, L., Jia, Y., 2012. Spatial variation in arsenic and fluoride concentrations of shallow groundwater from the town of Shahai in the Hetao basin, Inner Mongolia. Appl. Geochem. 27, 2187–2196.
Guo, Y., Yang, J., Zhang, Z., Li, G., Ting, L., Wang, L., 2021. Hydrogen and Oxygen Isotope Characteristics of Mine Water in the Shendong Mine Area and Water-rock Reactions Mechanism of the Formation of High-fluoride Mine Water. J. China Coal Soc.
Hao, C., Huang, Y., He, P., Sun, W., 2019. Isotope drift characteristics in ordovician limestone karst water caused by coal mining in Northern China. Mine Water Environ.
Hao, C., Zhang, W., Gui, H., 2020b. Hydrogeochemistry characteristic contrasts between low- and high-antimony in shallow drinkable groundwater at the largest antimony mine in hunan province, China. Appl. Geochem. 117, 104584.
Hao, C., Zhang, W., Gui, H., 2021a. Geochemical behaviours and formation mechanisms for elevated fluoride in the drinking groundwater in sulin coal-mining District, Northern Anhui Province, China. Pol. J. Environ. Stud. 30, 3565–3578.
Hao, C., Zhang, W., He, R., 2021b. Formation mechanisms for elevated fluoride in the mine water in Shendong coal-mining district. J. China Coal Soc. 46, 1966–1977.
Hao, C.-M., Huang, Y., Ma, D.-J., Fan, X., 2020a. Hydro-geochemistry evolution in Ordovician limestone water induced by mountainous coal mining: a case study from North China. J. Mt. Sci. Engl. 17, 614–623.
He, J., An, Y., Zhang, F., 2013a. Geochemical characteristics and fluoride distribution in the groundwater of the Zhangye Basin in Northwestern China. J. Geochem. Explor. 135, 22–30.
He, X., Ma, T., Wang, Y., 2013b. Hydrogeochemistry of high fluoride groundwater in shallow aquifers, Hangjinhouqi, Hetao Plain. J. Geochem. Explor. 135, 63–70.
Heaton, T.H.E., 1986. Isotopic studies of nitrogen pollution in the hydrosphere and atmosphere: a review. Chem. Geol. Isot. Geosci. Sect. 59, 87–102.
Jacks, G., Bhattacharya, P., Chaudhary, V., Singh, K.P., 2005. Controls on the genesis of some high-fluoride groundwaters in India. Appl. Geochem. 20, 221–228.
Kalpana, L., Brindha, K., Elango, L., 2019. FIMAR: a new fluoride index to mitigate geogenic contamination by managed aquifer recharge. Chemosphere 220, 381–390.
Kaur, L., Rishi, M.S., Sharma, S., Sharma, B., Lata, R., Singh, G., 2019. Hydrogeochemical characterization of groundwater in alluvial plains of river Yamuna in northern India: An insight of controlling processes. J. King Saud. Univ. - Sci.
Kefeni, K.K., Msagati, T.A.M., Mamba, B.B., 2017. Acid mine drainage: Prevention, treatment options, and resource recovery: a review. J. Clean. Prod. 151, 475–493.
Kim, D.-M., Yun, S.-T., Yoon, S., Mayer, B., 2019. Signature of oxygen and sulfur isotopes of sulfate in ground and surface water reflecting enhanced sulfide oxidation in mine areas. Appl. Geochem. 100, 143–151.
Kim, K., Rajmohan, N., Kim, H.J., Hwang, G.-S., Cho, M.J., 2004. Assessment of groundwater chemistry in a coastal region (Kunsan, Korea) having complex contaminant sources: a stoichiometric approach. Environ. Geol. 46, 763–774.
Knappett, P.S.K., Li, Y., Hernandez, H., Rodriguez, R., Aviles, M., Deng, C., Pina, V., Giardino, J.R., Mahlknecht, J., Datta, S., 2018. Changing recharge pathways within an intensively pumped aquifer with high fluoride concentrations in Central Mexico. Sci. Total. Environ. 622–623, 1029–1045.
Kornexl, B.E., Gehre, M., Höffling, R., Werner, R.A., 1999. On-line d18O measurement of organic and inorganic substances. Rapid Commun. Mass Sp. 13, 1685–1693.
Kumar, P., Singh, C.K., Saraswat, C., Mishra, B., Sharma, T., 2019. Evaluation of aqueous geochemistry of fluoride enriched groundwater: a case study of the Patan district, Gujarat, Western India. Water Sci. 31, 215–229.
Kumar, S., Venkatesh, A.S., Singh, R., Udayabhanu, G., Saha, D., 2018. Geochemical signatures and isotopic systematics constraining dynamics of fluoride contamination in groundwater across Jamui district, Indo-Gangetic alluvial plains, India. Chemosphere 205, 493–505.
LaFayette, G.N., Knappett, P.S.K., Li, Y., Loza-Aguirre, I., Polizzotto, M.L., 2020. Geogenic sources and chemical controls on fluoride release to groundwater in the Independence Basin, Mexico. Appl. Geochem. 123, 104787.
Li, C., Gao, X., Wang, Y., 2015. Hydrogeochemistry of high-fluoride groundwater at Yuncheng Basin, northern China. Sci. Total Environ. 508, 155–165.

Li, C., Hao, C., Zhang, W., Gui, H., 2020. High antimony source and geochemical behaviors in mine drainage water in china's largest antimony mine. Pol. J. Environ. Stud. 29, 3663–3673.
Li, D., Gao, X., Wang, Y., Luo, W., 2018. Diverse mechanisms drive fluoride enrichment in groundwater in two neighboring sites in northern China. Environ. Pollut. 237, 430–441.
Li, Q., Ju, Y., Lu, W., Wang, G., Neupane, B., Sun, Y., 2016. Water-rock interaction and methanogenesis in formation water in the southeast Huaibei coalfield, China. Mar. Pet. Geol. 77, 435–447.
Li, Y., Bi, Y., Mi, W., Xie, S., Ji, L., 2021. Land-use change caused by anthropogenic activities increase fluoride and arsenic pollution in groundwater and human health risk. J. Hazard. Mater. 406, 124337.
Liu, Futian, 2008. Research on Groundwater Circulation and Hydrochemical Transport in the Northern Part Ordos Cretaceous Basin Based on Isotope Technology. Jilin University, Changchun.
Mao, R., Guo, H., Jia, Y., 2016. Distribution characteristics and genesis of flouoride groundwater in the Hetao basin,Inner Mongoli. Earth Sci. Front. 23, 260–268.
Mondal, D., Gupta, S., Reddy, D.V., Nagabhushanam, P., 2014. Geochemical controls on fluoride concentrations in groundwater from alluvial aquifers of the Birbhum district, West Bengal, India. J. Geochem. l Explor. 145, 190–206.
Morrison, J., Brockwell, T., Merren, T., Fourel, F., Phillips, A.M., 2001. On-line high precision stable hydrogen isotopic analyses on nanoliter water samples. Anal. Chem. 73, 3570–3575.
Nariyan, E., Wolkersdorfer, C., Sillanpaa, M., 2018. Sulfate removal from acid mine water from the deepest active European mine by precipitation and various electrocoagulation configurations. J. Environ. Manag. 227, 162–171.
Olaka, L.A., Wilke, F.D., Olago, D.O., Odada, E.O., Mulch, A., Musolff, A., 2016. Groundwater fluoride enrichment in an active rift setting: Central Kenya Rift case study. Sci. Total Environ. 545–546, 641–653.
Palma, P., Lopez-Orozco, R., Mourinha, C., Oropesa, A.L., Novais, M.H., Alvarenga, P., 2019. Assessment of the environmental impact of an abandoned mine using an integrative approach: a case-study of the "Las Musas" mine (Extremadura, Spain). Sci. Total Environ. 659, 84–94.
Pingping, K., Peng, L., Fuqiang, W., 2019. Use of multiple isotopes to evaluate the impact of mariculture on nutrient dynamics in coastal groundwater. Environ. Sci. Pollut. Res. Int. 26, 12399–12411.
Rafique, T., Naseem, S., Ozsvath, D., Hussain, R., Bhanger, M.I., Usmani, T.H., 2015. Geochemical controls of high fluoride groundwater in Umarkot Sub-District, Thar Desert, Pakistan. Sci. Total Environ. 530–531, 271–278.
Rashid, A., Guan, D.X., Farooqi, A., Khan, S., Zahir, S., Jehan, S., Khattak, S.A., Khan, M. S., Khan, R., 2018. Fluoride prevalence in groundwater around a fluorite mining area in the flood plain of the River Swat, Pakistan. Sci. Total Environ. 635, 203–215.
Rashid, A., Farooqi, A., Gao, X., Zahir, S., Noor, S., Khattak, J.A., 2020. Geochemical modeling, source apportionment, health risk exposure and control of higher fluoride in groundwater of sub-district Dargai, Pakistan. Chemosphere 243, 125409.
Salcedo Sánchez, E.R., Garrido Hoyos, S.E., Esteller, M.V., Martínez Morales, M., Ocampo Astudillo, A., 2017. Hydrogeochemistry and water-rock interactions in the urban area of Puebla Valley aquifer (Mexico). J. Geochem. Explor. 181, 219–235.
Samborska, K., Halas, S., 2010. 34S and 18O in dissolved sulfate as tracers of hydrogeochemical evolution of the Triassic carbonate aquifer exposed to intense groundwater exploitation (Olkusz–Zawiercie region, southern Poland). Appl. Geochem. 25, 1397–1414.
Schoeller, 1965. Hydrodynamique dans le karst [Hydrodynamics of karst]. Actes du Colloques de Doubronik. IAHS/UNESCO, Wallingford, UK and Paris, France, pp. 3–20.
Shao, S., Ma, B., Chen, Y., Zhang, W., Wang, C., 2021. Behavior and mechanism of fluoride removal from aqueous solutions by using synthesized CaSO4·2H2O nanorods. Chem. Eng. J. 426, 131364.
Sharma, S.K., Subramanian, V., 2008. Hydrochemistry of the Narmada and Tapti Rivers, India. Hydro. Process 22, 3444–3455.
Singh, A.K., Mahato, M.K., Neogi, B., Mondal, G.C., Singh, T.B., 2011. Hydrogeochemistry, elemental flux, and quality assessment of mine water in the pootkee-balihari mining area, Jharia Coalfield, India. Mine Water Environ. 30.
Song, H., Xu, J., Fang, J., Cao, Z., Yang, L., Li, T., 2020. Potential for mine water disposal in coal seam goaf: investigation of storage coefficients in the Shendong mining area. J. Clean. Prod. 244, 118646.
Su, H., Kang, W., Li, Y., Li, Z., 2021. Fluoride and nitrate contamination of groundwater in the Loess Plateau, China: Sources and related human health risks. Environ. Pollut. 286, 117287.
Sun, J., Kobayashi, T., Strosnider, W.H.J., Wu, P., 2017. Stable sulfur and oxygen isotopes as geochemical tracers of sulfate in karst waters. J. Hydrol. 551, 245–252.
Temovski, M., Futó, I., Túri, M., Palcsu, L., 2018. Sulfur and oxygen isotopes in the gypsum deposits of the Provalata sulfuric acid cave (Macedonia). Geomorphology 315, 80–90.
Thapa, R., Gupta, S., Gupta, A., Reddy, D.V., Kaur, H., 2018. Geochemical and geostatistical appraisal of fluoride contamination: an insight into the Quaternary aquifer. Sci. Total Environ. 640–641, 406–418.
Toolabi, A., Bonyadi, Z., Paydar, M., Najafpoor, A.A., Ramavandi, B., 2021. Spatial distribution, occurrence, and health risk assessment of nitrate, fluoride, and arsenic in Bam groundwater resource, Iran. Groundw. Sustain. Dev. 12, 100543.
Wang, H., Jiang, X.-W., Wan, L., Han, G., Guo, H., 2015. Hydrogeochemical characterization of groundwater flow systems in the discharge area of a river basin. J. Hydrol. 527, 433–441.
Wang, Z., Guo, H., Xiu, W., Wang, J., Shen, M., 2018. High arsenic groundwater in the Guide basin, northwestern China: distribution and genesis mechanisms. Sci. Total Environ. 640–641, 194–206.
Wen, B., Zhou, J., Zhou, A., Liu, C., Xie, L., 2016. Sources, migration and transformation of antimony contamination in the water environment of Xikuangshan, China: evidence from geochemical and stable isotope (S, Sr) signatures. Sci. Total Environ. 569–570, 114–122.
WHO, 1984. Guidelines for Drinking Water Quality. World Health Organization 2, Geneva.
Wu, C., Wu, X., Qian, C., Zhu, G., 2018. Hydrogeochemistry and groundwater quality assessment of high fluoride levels in the Yanchi endorheic region, northwest China. Appl. Geochem. 98, 404–417.
Xiao, W., Lv, X., Zhao, Y., Sun, H., Li, J., 2020. Ecological resilience assessment of an arid coal mining area using index of entropy and linear weighted analysis: a case study of Shendong Coalfield, China. Ecol. Indic. 109, 105843.
Xie, Q., Zhang, Z., Hou, T., Jin, Z., Santosh, M., 2017. Geochemistry and oxygen isotope composition of magnetite from the Zhangmatun deposit, North China Craton: implications for the magmatic-hydrothermal evolution of Cornwall-type iron mineralization. Ore Geol. Rev. 88, 57–70.
Xu, J., Zhu, W., Xu, J., Wu, J., Li, Y., 2021. High-intensity longwall mining-induced ground subsidence in Shendong coalfield, China. Int. J. Rock. Mech. Min. Sci. 141, 104730.
Yadav, K., Raphi, M., Jagadevan, S., 2021. Geochemical appraisal of fluoride contaminated groundwater in the vicinity of a coal mining region: spatial variability and health risk assessment. Geochemistry 81, 125684.
Yan, J., Chen, J., Zhang, W., Ma, F., 2020. Determining fluoride distribution and influencing factors in groundwater in Songyuan, Northeast China, using hydrochemical and isotopic methods. J. Geochem. Explor. 217, 106605.
Yao, G., 2017. The concentrations of F-, Cl- and SO42- determined by ion chromatography in drinking water of Shendong mining area. China Chem. Trade 9, 111–112.
Yousefi, M., Ghoochani, M., Hossein Mahvi, A., 2018. Health risk assessment to fluoride in drinking water of rural residents living in the Poldasht city, Northwest of Iran. Ecotoxicol. Environ. Saf. 148, 426–430.
Zango, M.S., Pelig-Ba, K.B., Anim-Gyampo, M., Gibrilla, A., Sunkari, E.D., 2021. Hydrogeochemical and isotopic controls on the source of fluoride in groundwater within the Vea catchment, northeastern Ghana. Groundw. Sustain. Dev. 12, 100526.
Zhang, D., Fan, G., Ma, L., Wang, X., 2011. Aquifer protection during longwall mining of shallow coal seams: A case study in the Shendong Coalfield of China. Int. J. Coal Geol. 86, 190–196.
Zhang, Q., Xu, P., Qian, H., Yang, F., 2020. Hydrogeochemistry and fluoride contamination in Jiaokou Irrigation District, Central China: assessment based on multivariate statistical approach and human health risk. Sci. Total Environ. 741, 140460.
Zhang, S., Liu, G., Sun, R., Wu, D., 2016. Health risk assessment of heavy metals in groundwater of coal mining area: a case study in Dingji coal mine, Huainan coalfield, China. Hum. Ecol. Risk Assess.: Int. J. 22, 1469–1479.
Zhang, Z., Li, G., Su, X., Zhuang, X., Wang, L., Fu, H., Li, L., 2021. Geochemical controls on the enrichment of fluoride in the mine water of the Shendong mining area, China. Chemosphere 284, 131388.
Zhao, B., Wei, N., 2020. Study on content distribution and occurrenceform of fluorine in Shaanxi coal. Coal Qual. Technol. 35, 34–39.
Zhong, B., Wang, L., Liang, T., Xing, B., 2017. Pollution level and inhalation exposure of ambient aerosol fluoride as affected by polymetallic rare earth mining and smelting in Baotou, north China. Atmos. Environ. 167, 40–48.
Zhou, J., Zhang, Q., Kang, F., Zhang, Y., Yuan, L., Wei, D., Lin, S., 2018. Using multi-isotopes (^{34}S, ^{18}O, ^{2}H) to track local contamination of the groundwater from Hongshan-Zhaili abandoned coal mine, Zibo city, Shandong province. Int. Biodeter. Biodegr. 128, 48–55.

Further reading

Blasco, M., Auqué, L.F., Gimeno, M.J., 2019. Geochemical evolution of thermal waters in carbonate – evaporitic systems: the triggering effect of halite dissolution in the dedolomitisation and albitisation processes. J. Hydrol. 570, 623–636.
Gaofeng, Z., Yonghong, S., Chunlin, H., Qi, F., Zhiguang, L., 2009. Hydrogeochemical processes in the groundwater environment of Heihe River Basin, northwest China. Environ. Earth Sci. 60, 139–153.
Guan, Q., Wang, L., Wang, F., Pan, B., Song, N., Li, F., Lu, M., 2016. Phosphorus in the catchment of high sediment load river: a case of the Yellow River, China. Sci. Total Environ. 572, 660–670.
Brintzinger, H., 1948. Die Antimonat-, Antimonit-, Germanat- und Aluminat-lonen im gelösten Zustand. Z. Anorg. Allg. Chem. 256, 98–102.
Pi, K., Wang, Y., Xie, X., Su, C., Ma, T., Li, J., Liu, Y., 2015. Hydrogeochemistry of co-occurring geogenic arsenic, fluoride and iodine in groundwater at Datong Basin, northern China. J. Hazard. Mater. 300, 652–661.
Piper, M., 1944. Graphic Procedure in the Geochemical Interpretation of Water-analyses. Hydrology 914–928.
Xiangquan, L., Liren, Z., Xinwei, H., 2007. Distribution and evolutional mechanism of shallow High_FluorideGroundwater in Taiyuan Basin. Acta Geosci. Sin. 28, 55–61.
Xiao, J., Jin, Z., Zhang, F., 2015. Geochemical controls on fluoride concentrations in natural waters from the middle Loess Plateau, China. J. Geochem. Explor. 159, 252–261.
Yang, J., Dong, S., Wang, H., Li, G., Wang, T., Wang, Q., 2020. Mine water source discrimination based on hydrogeochemical characteristics in the Northern Ordos Basin, China. Mine Water Environ. 40, 433–441.